UCLA
UCLA Previously Published Works

Title
Semi-analytical modeling of anchor loss in plate-mounted resonators.

Permalink
https://escholarship.org/uc/item/9q88b2v0

Authors
Schaal, Christoph
M'Closkey, Robert
Mal, Ajit

Publication Date
2018

DOI
10.1016/j.ultras.2017.09.009

Peer reviewed

eScholarship.org Powered by the California Digital Library
University of California

Semi-analytical modeling of anchor loss in plate-mounted resonators

Christoph Schaal[a,b,*], Robert M'Closkey[b], Ajit Mal[b]

[a] *Department of Mechanical Engineering, California State University, Northridge, California, USA*
[b] *Mechanical and Aerospace Engineering Department, University of California, Los Angeles, California, USA*

Abstract

A semi-analytical technique for estimating the energy loss in a resonator mounted to an infinite plate substrate is proposed in this paper. In a plate, only Lamb waves have to be considered, leading to a simplified characterization of the energy carried away from a vibrating source on the plate surface. Instead of employing absorbing elements at the boundaries of the plate-resonator finite element model, it is shown how the semi-analytical approach of stitching together analytical Lamb wave expressions to the finite element model can be utilized. The approach is demonstrated for single and double cantilever configurations on a plate. The results have excellent agreement with those of conventional transient finite element simulations.
Keywords: Micro-resonator, anchor loss, Lamb waves, semi-analytical, FEM

1. Introduction

Damping in miniature resonators (e.g. vibratory gyroscopes) is a consequence of many factors and for the designer of such devices it is important to determine the dominant mechanisms that contribute to energy loss [1]. Energy loss in a vibratory gyroscope due to the interaction with the substrate to which it is mounted, commonly termed *anchor loss*, has been widely studied [2–4]. Most treatments, however, have assumed a semi-infinite medium due to the small dimensions of the resonator compared to the substrate thickness [5]. Recently reported high quality factor resonators, though, typically have resonant frequencies from a few kilohertz up to several hundred kilohertz [6–9, 4], and due to the wavelengths involved, the substrate is more accurately treated as a plate, not as a semi-infinite medium. These substrate plates are often made of fused silica or Pyrex glass and can therefore be treated as an isotropic medium [9, 10]. In any case, it is common practice to create a model of the resonator that includes a small segment of the plate with a finite element (FE) software in conjunction with absorbing boundary elements [11, 5]. As an alternative to implementing absorbing boundary elements, semi-analytical methods have been developed in which such elements are replaced by analytical expressions for Lamb waves [12]. By means of a modal superposition of all possible Lamb waves, any displacement and stress field can be represented due to the

*Corresponding author

fact that Lamb waves form a complete set [13]. Such semi-analytical methods have been successfully applied to investigate Lamb wave-scattering from damaged areas using FE models [14, 15] and boundary element (BE) models [16], and can also be applied here. The semi-analytical approach requires the specification of a harmonic load and the determination of the subsequent harmonic response at a point on the resonator. The modal frequency and damping can be estimated from the frequency response function (FRF) that has been computed on a frequency grid. The solution of transient problems can be obtained through inversion of the frequency domain solution using IFFT codes.

Extensive research has been conducted on the propagation of Lamb waves in isotropic and anisotropic plates [17–21]. Mal and Lih [22] and Lih and Mal [23] have derived the exact solution of three-dimensional problems, consisting of multi-layered, angle-ply laminates of finite thickness and large lateral dimensions that are subject to various types of surface loads. Approximate thin-plate theories have also been developed to obtain the analytical solutions for the response of thin isotropic and anisotropic plates to surface loads [24]. However, the derivation of the expressions for the sources created in the support region by the resonator motion can be challenging to determine [25]. Other semi-analytical methods, such as the distributed point source method (DPSM) [26], have recently been developed extend the scope of such analyses.

This paper revisits the previously described semi-analytical approach, in which an external load is artificially applied to the resonator for purpose of computing the FRF. The resonator and a small section of the substrate plate are discretized using standard FE methods, and then analytical expressions are used to apply appropriate boundary conditions according to the Lamb wave theory. The resulting overdetermined system of linear equations can be solved in a least-square sense. A wave and finite element (WFE) approach [27, 28] is used to determine the required roots of the Lamb wave dispersion equations. It should be noted that the WFE-based approach can also be applied to more complex anisotropic structural components [21, 29]. Alternatively, the spectral finite element (SFE) method [30, 31] can also be used to determine these roots. Without loss of generality, only two dimensional problems are considered in this paper. The idea is first demonstrated on a single cantilever attached to an elastic plate. For high quality factor resonators with minimal material damping and anchor loss, transient simulations become impractical and alternative methods are required for estimating the apparent damping in the resonator. Hence, a second case is investigated with the semi-analytical method in order to demonstrate its feasibility for the case of two cantilevers located in close proximity to each other.

The paper is organized as follows. A motivating example consisting of a discrete undamped spring-mass resonator attached to a semi-infinite beam is discussed in Section 2. The frequency response of the mass position due to a harmonic force applied to the mass has a closed form solution. In Section 3, the semi-analytical methods to solve the more realistic case of a resonator attached to an elastic plate are presented. The fundamentals of guided ultrasonic wave propagation in plates are briefly reviewed in Section 3.1. The semi-analytical frequency response method for the given class of problems is formulated in Section 3.2. In

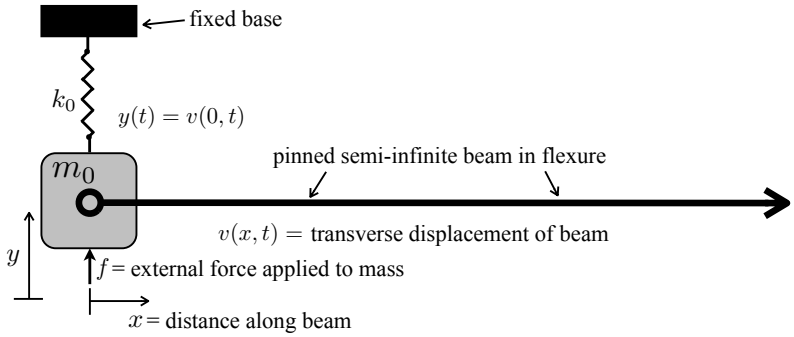

Figure 1: Discrete spring-mass system pinned to a semi-infinite beam

Section 4, the semi-analytical method is applied to cantilever beam resonators in various configurations. Additionally, results are also obtained from transient FE simulations. Some observations and discussion are given in Section 5, and Section 6 presents concluding remarks.

2. Motivating example

In this section, an example is considered for which the semi-analytical steady-state frequency response analysis can be determined in closed-form. The model is a semi-infinite beam which is coupled at one end to a spring-mass subsystem, as shown in Fig. 1. The spring (spring constant k_0) and discrete mass m_0 represent a lossless subsystem, which is coupled to the beam with a pin joint (zero moment). The beam is assumed to have m_b mass per unit length, Young's modulus E and cross-sectional moment of inertia I.

For low frequencies, the dynamics of this system are described by the Euler-Bernoulli beam equation

$$a^2 \frac{\partial^4 v}{\partial x^4} + \ddot{v} = 0\,, \quad a = \sqrt{\frac{EI}{m_\mathrm{b}}} \tag{1}$$

with the boundary conditions

$$m_0 \ddot{y} = -k_0 y + f - EI \left.\frac{\partial^3 v}{\partial x^3}\right|_{x=0} \quad \text{and} \quad \left.\frac{\partial^2 v}{\partial x^2}\right|_{x=0} = 0\,, \tag{2}$$

where v represents the transverse displacement of the beam, $x \geq 0$ is the distance along the beam, and y is the displacement of the discrete mass ($y(t) = v(0,t)$).

Assuming beam motion of the form $e^{\mathrm{i}(kx-\omega t)}$, yields the beam dispersion relation $k^4 = \omega^2/a^2$. Two wavenumbers are of physical relevance to this problem when $\omega > 0$: a real, positive solution $k_1 = \sqrt{\omega/a}$ that represents a right-propagating wave ($x \to +\infty$), and another positive imaginary solution $k_2 = \mathrm{i}\sqrt{\omega/a}$ that represents a decaying non-propagating wave. In order to determine the frequency response of the discrete mass, the external force is defined as the harmonic function $f(t) = \mathrm{e}^{-\mathrm{i}\omega t}$. The function

$$v(x,t) = u_1\, \mathrm{e}^{\mathrm{i}(k_1 x - \omega t)} + u_2\, \mathrm{e}^{\mathrm{i}(k_2 x - \omega t)} \tag{3}$$

satisfies the beam equation and $u_1, u_2 \in \mathbb{C}$ are constants to be determined such that this solution is also consistent with the mass motion and zero-moment interface conditions. This yields the expression

$$\underbrace{\begin{bmatrix} -\omega^2 m_0 + k_0 - \mathrm{i}EIk_1^3 & -\omega^2 m_0 + k_0 - \mathrm{i}EIk_2^3 \\ k_1^2 & k_2^2 \end{bmatrix}}_{\boldsymbol{D}(\omega)} \underbrace{\begin{bmatrix} u_1 \\ u_2 \end{bmatrix}}_{\boldsymbol{u}} = \begin{bmatrix} 1 \\ 0 \end{bmatrix} , \tag{4}$$

from which $\{u_1, u_2\}$ are determined to be

$$u_1 = u_2 = \frac{\frac{1}{2}}{-\omega^2 m_0 + k_0 - \frac{1}{2}EI\frac{\omega}{a}\sqrt{\frac{\omega}{a}}\,(1+i)} .$$

The harmonic beam response is

$$v(x,t) = \frac{\frac{1}{2}\left(e^{\mathrm{i}k_1 x} + e^{\mathrm{i}k_2 x}\right)}{-\omega^2 m_0 + k_0 - \frac{1}{2}EI\frac{\omega}{a}\sqrt{\frac{\omega}{a}}\,(1+\mathrm{i})} e^{-\mathrm{i}\omega t} ,$$

and the discrete mass response is

$$y(t) = v(0,t) = \frac{1}{-\omega^2 m_0 + k_0 - \frac{1}{2}EI\frac{\omega}{a}\sqrt{\frac{\omega}{a}}\,(1+\mathrm{i})} e^{-\mathrm{i}\omega t} . \tag{5}$$

Due to the phase of the harmonic forcing, the expression multiplying $e^{-\mathrm{i}\omega t}$ in Eq. (5) is the complex conjugate of the Fourier transform of the discrete mass impulse response. Thus, if h denotes the impulse response of the discrete mass, then the frequency response function associated with its position is

$$\mathcal{F}(h) = \frac{1}{-\omega^2 m_0 + k_0 - \frac{1}{2}EI\frac{\omega}{a}\sqrt{\frac{\omega}{a}}\,(1-i)} , \tag{6}$$

where $\mathcal{F}(\cdot)$ is the Fourier transform operator.

The magnitude and phase of the FRF in Eq. (6) are shown in Fig. 2(a) when the model parameters are selected as $EI = 1\,\mathrm{Nm}^2$, $a = 1\,\mathrm{m}^2/\mathrm{s}$, $k_0/m_0 = 1\,1/\mathrm{s}^2$, $m_\mathrm{b} = 1\,\mathrm{kg/m}$ and $m_0 = 2\,\mathrm{kg}$. These parameters are selected for illustrative purposes and are not intended to model a physical system. The inverse Fourier transform of Eq. (6) is numerically approximated and yields the impulse response h, shown in Fig. 2(b) (numerically approximated). This analysis is analogous to the well-established semi-analytical approach for studying the steady-state properties of plates and layered media in unbounded domains. In this example, the analytical expression for the wave motion in the beam, i.e. $v(x,t)$, is a proxy for the plate Lamb waves' expressions, and the discrete spring-mass system represents the discretized FE portion of the plate and attached resonator. For a harmonic force applied to the discrete spring-mass system, the amplitudes $\{u_1, u_2\}$ of the analytical expression for the beam are determined such that the discrete spring-mass motion matches that of the beam at their interface.

A typical approach to compute the apparent damping in the discrete mass position is to fit a single degree of freedom (SDOF) damped linear harmonic oscillator model to the FRF data shown in Fig. 2(a). An interesting feature of this example, though, which is also shared by the semi-analytical method applied

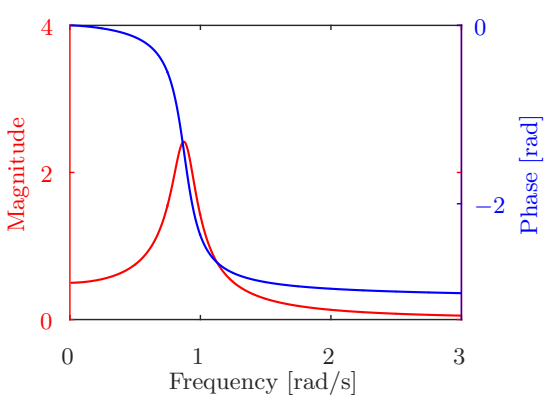

(a) Frequency response of the position of m_0

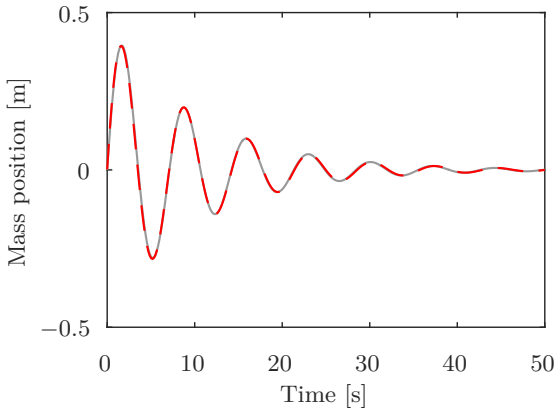

(b) Impulse response associated with the position of m_0 (red dashed); SDOF approximation (gray solid)

Figure 2: Response graphs for the discrete mass m_0 coupled to a semi-infinite beam

to plate problems, is the fact that the FRF is not a rational function of ω. Hence, attempts to estimate a "natural frequency" and associated "damping" from the magnitude and phase graphs (or time domain response) are necessarily approximations. Nevertheless, from a practical perspective, reasonable estimates can be obtained. For example, since the impulse response of a linear, damped SDOF system is given by $h_{\text{SDOF}}(t) = \alpha e^{-\sigma t}\sin(\tilde{\omega}t)\mathbb{1}(t)$, where $\mathbb{1}$ is the Heaviside step function, the parameters $\{\alpha, \sigma, \tilde{\omega}\}$ are determined so that the Euclidean norm of the difference between the numerically estimated impulse response of the mass-beam system and $h_{\text{SDOF}}(t)$ is minimized over a desired time interval. Here, these parameters are chosen to minimize $\sum_k (h(t_k) - h_{\text{SDOF}}(t_k))^2$, where the summation index k covers the time grid of the numerical estimate of $h(t)$ on the interval $[0, 100]$ s. This optimization yields the parameters $\alpha = 0.4676$, $\sigma = 0.0970$, and $\tilde{\omega} = 0.8841$. The graph of $h_{\text{SDOF}}(t)$ is shown as a solid gray line in Fig. 2(b) and is observed to be indistinguishable from the actual impulse response $h(t)$ (red dashed) on the displayed scale.

3. Analysis of resonators attached to plates

3.1. Ultrasonic wave propagation in plates

The fundamentals of ultrasonic wave propagation in plates are briefly reviewed in this section. Guided ultrasonic wave propagation in homogeneous isotropic plates as well as in more complex media, e.g. isotropic multi-layered plates, have been studied by numerous authors (e.g. [17, 18, 32]). More recently, theoretical and experimental studies in anisotropic media have also been carried out [20, 21]. Guided waves in homogeneous plates are called Lamb waves [12]. The characteristic equations for Lamb waves, denoted Δ_{a} for antisymmetric wave motion and Δ_{s} for symmetric wave motion, are well known and can be expressed in the

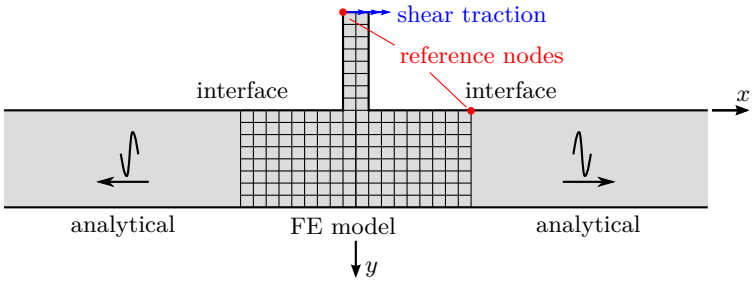

Figure 3: Frequency response approach: the resonator and a small segment of the substrate plate are modeled with finite elements. The resonator is harmonically loaded, and the response is determined for a given frequency range

form [33]

$$\Delta_{\mathrm{a}} = \left(2k^2 - k_2^2\right)^2 \sinh(\eta_1 H)\cosh(\eta_2 H) - 4k^2\eta_1\eta_2 \cosh(\eta_1 H)\sinh(\eta_2 H) = 0 \quad \text{and} \tag{7}$$

$$\Delta_{\mathrm{s}} = \left(2k^2 - k_2^2\right)^2 \cosh(\eta_1 H)\sinh(\eta_2 H) - 4k^2\eta_1\eta_2 \sinh(\eta_1 H)\cosh(\eta_2 H) = 0\,. \tag{8}$$

In above equations,

$$\eta_j = \sqrt{k^2 - k_j^2}\,, \quad k_j = \frac{\omega}{c_j}\,, \quad \text{for} \quad j = 1, 2\,, \tag{9}$$

where ω is the angular frequency, k is the wavenumber, H is half the plate thickness and c_1 and c_2 are the P- and S-wave speeds, respectively. For the sake of brevity, the general expressions for displacement and stress fields for symmetric and anti-symmetric Lamb waves are omitted here but can be found in the literature (e.g. [34]).

Solving for the real, imaginary and complex roots of the transcendental equations (7) and (8) is challenging, however, the necessity of having all these roots and their meaning has been addressed by various authors [35–37]. A number of so-called semi-analytical methods have recently been developed to determine the roots of the dispersion equations corresponding to propagating, non-propagating and evanescent Lamb waves in multi-layered waveguides [30, 31, 27]. In all of these methods, roots of Eqs. (7) and (8) are determined. In this paper, the wave and finite element (WFE) approach [27, 38, 28] is used to determine the real, imaginary and complex roots of the aforementioned dispersion equations due to the method's versatility

3.2. Frequency response analysis

A semi-analytical method is used to determine the harmonic response of a harmonically forced resonator mounted to a plate. A finite element (FE) model of the resonator and finite portion of the substrate plate is created as shown in Fig. 3 where, without loss of generality, a cantilever beam represents the resonator. Analytical Lamb wave expressions are matched to the nodal displacements and forces at the FE plate boundaries. Since a forcing mechanism is required in this analysis, the resonator is harmonically loaded, and the harmonic response at a reference node on the resonator is used as the "pick-off" in order create a FRF for the system.

The FE modeling process yields the dynamics of the resonator and plate segment, which are described by the equations of motion

$$\boldsymbol{M}\ddot{\boldsymbol{u}} + \boldsymbol{K}\boldsymbol{u} = \boldsymbol{f}\,, \tag{10}$$

where $\boldsymbol{M}$ and $\boldsymbol{K}$ are the mass and stiffness matrices, and $\boldsymbol{u}$ and $\boldsymbol{f}$ are the nodal displacement and forces, respectively. Note that material damping is not considered in this analysis. Assuming harmonic forcing of the form $\mathrm{e}^{-\mathrm{i}\omega t}$ with $\omega \in \mathbb{R}$, a harmonic particular solution can be determined from

$$\underbrace{\begin{bmatrix} \boldsymbol{D}_{\mathrm{II}} & \boldsymbol{D}_{\mathrm{IB}} \\ \boldsymbol{D}_{\mathrm{BI}} & \boldsymbol{D}_{\mathrm{BB}} \end{bmatrix}}_{\boldsymbol{D}} \begin{bmatrix} \boldsymbol{u}_{\mathrm{I}} \\ \boldsymbol{u}_{\mathrm{B}} \end{bmatrix} = \begin{bmatrix} \boldsymbol{f}_{\mathrm{I}} \\ \boldsymbol{f}_{\mathrm{B}} \end{bmatrix}\,, \tag{11}$$

where the dynamic stiffness matrix $\boldsymbol{D}$ is given by

$$\boldsymbol{D} = -\omega^2\boldsymbol{M} + \boldsymbol{K}. \tag{12}$$

The displacement and force arrays are arranged into two partitions: the subscripts I and B denote interior and boundary nodes, respectively. Although the inner degrees of freedom $\boldsymbol{u}_{\mathrm{I}}$ can be eliminated from Eq. (11) by applying

$$\boldsymbol{u}_{\mathrm{I}} = \boldsymbol{D}_{\mathrm{II}}^{-1}\left(\boldsymbol{f}_{\mathrm{I}} - \boldsymbol{D}_{\mathrm{IB}}\boldsymbol{u}_{\mathrm{B}}\right)\,, \tag{13}$$

this would involve a numerically costly inversion of the matrix $\boldsymbol{D}_{\mathrm{II}}$. Instead, the necessary inversion is performed on the boundary nodes as shown below.

At the boundary interfaces, continuity and equilibrium equations must hold between the FE and analytical models [14]:

$$\boldsymbol{u}_{\mathrm{ana}} = \boldsymbol{u}_{\mathrm{B}} \quad \text{and} \quad \boldsymbol{f}_{\mathrm{ana}} = -\boldsymbol{f}_{\mathrm{B}}\,. \tag{14}$$

Using the Lamb wave theory, analytical expressions for displacements $\boldsymbol{u}_{\mathrm{ana}}$ and tractions $\boldsymbol{t}_{\mathrm{ana}}$ can be written as a superposition of n_m modes

$$\boldsymbol{u}_{\mathrm{ana}} = \sum_{i=1}^{n_{\mathrm{m}}} \hat{\boldsymbol{u}}_i a_i = \hat{\boldsymbol{U}}\boldsymbol{a} \qquad \text{and} \qquad \boldsymbol{t}_{\mathrm{ana}} = \sum_{i=1}^{n_{\mathrm{m}}} \hat{\boldsymbol{t}}_i a_i = \hat{\boldsymbol{T}}\boldsymbol{a}\,, \tag{15}$$

where the columns of the matrices of modal displacements $\hat{\boldsymbol{U}}$ and tractions $\hat{\boldsymbol{T}}$ are composed of the corresponding mode shape vectors, i.e.

$$\hat{\boldsymbol{U}} = \begin{bmatrix} \hat{\boldsymbol{u}}_1 & \hat{\boldsymbol{u}}_2 & \dots & \hat{\boldsymbol{u}}_{n_{\mathrm{m}}} \end{bmatrix} \quad \text{and} \quad \hat{\boldsymbol{T}} = \begin{bmatrix} \hat{\boldsymbol{t}}_1 & \hat{\boldsymbol{t}}_2 & \dots & \hat{\boldsymbol{t}}_{n_{\mathrm{m}}} \end{bmatrix}\,. \tag{16}$$

The scalar unknown modal amplitudes a_i are dependent on any wave sources in the FEA model and are combined into the column matrix $\boldsymbol{a}$. The tractions are determined from the corresponding stresses $\boldsymbol{\sigma}$ (e.g. [34]) and the relation $\boldsymbol{t} = \boldsymbol{\sigma}\cdot\boldsymbol{n}$, where $\boldsymbol{n}$ is the normal vector of the corresponding boundary interface. The expressions for the displacements and stresses are typically given for right-propagating waves, i.e. waves

that propagate towards $+\infty$. Since waves through the left interface must propagate to the left (towards $-\infty$), the wavenumber k is replaced by $-k$ to transform the expression for right-propagating waves into the appropriate counterparts for left-propagating waves. It is also worth mentioning that other truncations of the infinite sums in Eq. (15) might be desirable for other problems [39, 40]. In order to satisfy Eq. (14), the analytical expressions are evaluated at spatially discretized nodes that correspond to the nodes of the FE model. Furthermore, tractions $\hat{\boldsymbol{t}}$ are converted into nodal forces $\hat{\boldsymbol{f}}$ via a common integration technique using shape functions.

Combining the expressions from Eqs. (14) and (15), writing tractions in the form of nodal forces ($\hat{\boldsymbol{t}} \rightarrow \hat{\boldsymbol{f}}$ and $\hat{\boldsymbol{T}} \rightarrow \hat{\boldsymbol{F}}$), and noting that $\hat{\boldsymbol{U}}$ has full column rank allows the nodal forces at the FE-analytical boundary to be written in terms of the wave amplitudes at the boundary nodes

$$\boldsymbol{f}_{\mathrm{B}} = \hat{\boldsymbol{F}}\hat{\boldsymbol{U}}^{\dagger}\boldsymbol{u}_{\mathrm{B}}\,, \tag{17}$$

where $\hat{\boldsymbol{U}}^{\dagger}$ denotes the Moore-Penrose generalized-inverse of $\hat{\boldsymbol{U}}$. Substituting Eq. (17) into Eq. (11) and rearranging yields

$$\underbrace{\begin{bmatrix} \boldsymbol{D}_{\mathrm{II}} & \boldsymbol{D}_{\mathrm{IB}} \\ \boldsymbol{D}_{\mathrm{BI}} & \boldsymbol{D}_{\mathrm{BB}} - \hat{\boldsymbol{F}}(\omega)\hat{\boldsymbol{U}}^{\dagger}(\omega) \end{bmatrix}}_{\boldsymbol{D}_a(\omega)} \begin{bmatrix} \boldsymbol{u}_{\mathrm{I}} \\ \boldsymbol{u}_{\mathrm{B}} \end{bmatrix} = \begin{bmatrix} \boldsymbol{f}_{\mathrm{I}}(\omega) \\ \boldsymbol{0} \end{bmatrix}, \quad \omega \in \mathbb{R}\,, \tag{18}$$

where $\boldsymbol{D}_a(\omega)$ is the *augmented* dynamic stiffness matrix. The fact that the generalized-inverse of $\hat{\boldsymbol{U}}$ is used is a well-established practice for this purpose [41]. The only non-zero entries in the array $\boldsymbol{f}_{\mathrm{I}}$ of nodal forces at interior nodes correspond to the external excitation of the resonator. Assuming a sufficiently fine discretization of the FE model, Eq. (18) is an overdetermined system of linear equations for which a least-squares solution is determined for each frequency of interest. The solution $[\boldsymbol{u}_{\mathrm{I}}\ \boldsymbol{u}_{\mathrm{B}}]^{\mathrm{T}}$ is calculated at every node and frequency response functions are thus determined.

4. Numerical results

In the following, the semi-analytical methods are applied to two problems: a cantilever beam mounted on a substrate plate in Section 4.1 (see Fig. 4(a)), and a double cantilever problem in Section 4.2 (see Fig. 4(b)). The resonator-plate system is assumed to follow homogeneous, isotropic, linearly elastic material behavior. Plane-strain FE models are implemented in the software package Abaqus and post-processing is performed in Matlab. To this end, the interface conditions between the numerical and analytical domains are implemented after importing nodal information and global mass and stiffness matrices into Matlab. For the FE model, 4-node bilinear elements (CPE4) are used with a spatial resolution of about 0.1 mm, which is over 40 times smaller than the smallest wave length of the Lamb waves in the considered frequency range. For the FRF analysis, the resonator is harmonically loaded at all nodes on the top edge, and the harmonic

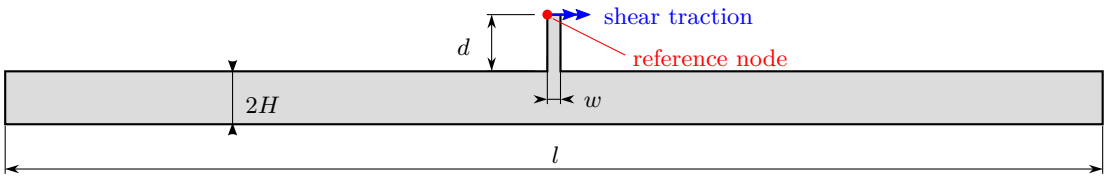

(a) Single cantilever

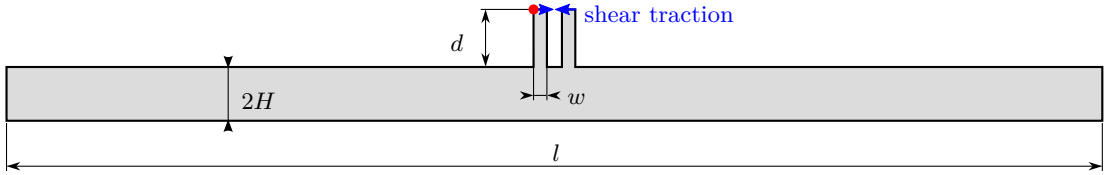

(b) Double cantilever (symmetric loading shown)

Figure 4: Scale figures of the FE models used in semi-analytical methods. Loading is only applied for determining the FRF at reference node

response is determined at the reference node. Transient FE simulations are also performed in both cases for comparison to the steady-state analysis results.

4.1. Single Cantilever

Consider a cantilever (length $d = 1.906\,\text{mm}$, thickness $w = 0.445\,\text{mm}$) that is bonded to a substrate plate segment (thickness $2H = 1.78\,\text{mm}$, $l = 20\,\text{mm}$) of the same material (aluminum, Young's modulus $E = 69\,\text{GPa}$, shear modulus $G = 26\,\text{GPa}$, density $\rho = 2700\,\text{kg/m}^3$), as shown in Fig. 4(a). This system will first be analyzed for its frequency response according to Section 3.2. A uniform shear traction in the x-direction is applied to all nodes on the top edge of the cantilever while all other interior nodes are unforced. The WFE method is used to compute the necessary wavenumbers for the propagating, non-propagating and evanescent waves for frequencies between 50 kHz and 500 kHz. For example, the wavenumbers for $f = 100\,\text{kHz}$ are shown in Fig. 5. The two relevant real roots are denoted by $\times$, the imaginary root by $+$ and complex roots are marked by $\bullet$.

For the considered plate segment, the interfaces between the FE and analytical domain are about six plate thicknesses away from the cantilever "source," and only nine roots (real, imaginary and complex) are retained for the analysis. The corresponding mode shape vectors form $\hat{\boldsymbol{U}}$ and $\hat{\boldsymbol{F}}$ so that Eq. (18) can be solved. Magnitude and phase of the solution of Eq. (18) for this problem are shown as solid lines in Fig. 6(a). The maximum amplitude is located at $f = 83.7\,\text{kHz}$, and this eigenfrequency corresponds to the first eigenmode of the cantilever coupled to the substrate plate. The damping is approximated as 14.1 1/s based on the fit of an SDOF model to the FRF data, minimizing the Euclidean norm of the differences. Referring to the example in Section 2, the frequency response function is not a rational function of ω, so the fit can only be achieved in an approximate sense. Note that the non-zero damping value indicates that this mode shape, corresponding to what would be considered the first bending mode of the cantilever,

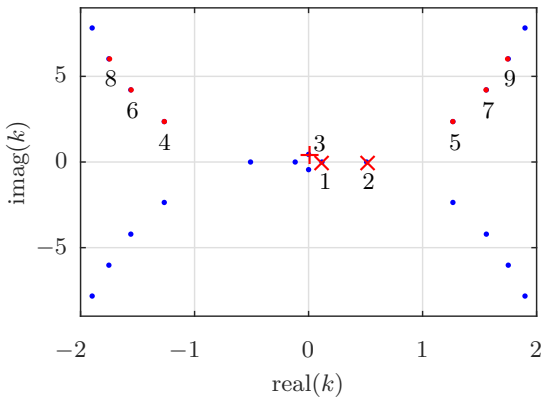

Figure 5: Complex roots (unit [rad/mm]) of the dispersion equations for an aluminum substrate plate with $2H = 1.78\,\text{mm}$ at $f = 100\,\text{kHz}$. Considered modes in semi-analytical approach are highlighted in red

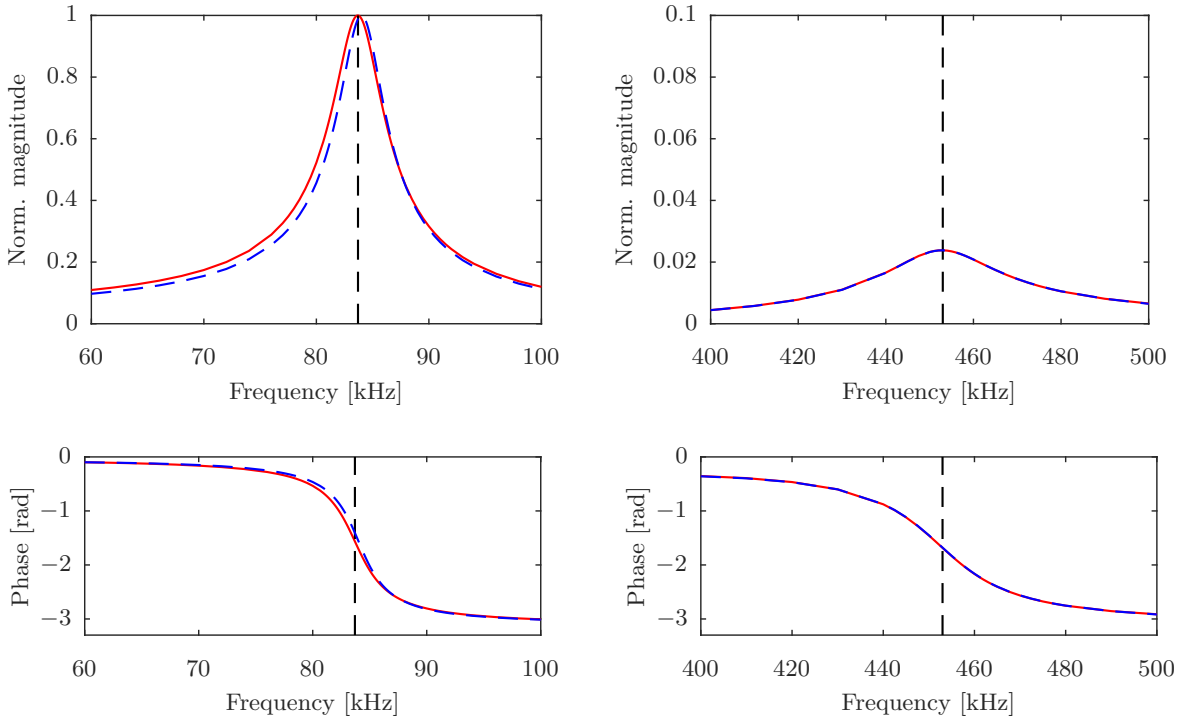

(a) FRF near first peak

(b) FRF near second peak

Figure 6: FRFs at reference node for single cantilever problem. Solid lines correspond to the $l = 20\,\text{mm}$ model and dashed lines denote results for the $l = 10\,\text{mm}$ model. Magnitudes are normalized to maximum value

experiences damping due to the energy transport of the propagating Lamb waves in the substrate plate [25]. The frequency of this damped mode is lower than the frequency of the cantilever's first bending mode when it is fixed to a rigid inelastic substrate. The FRF near the second eigenmode is also shown in Fig. 6(b) and it is observed that the apparent damping of this mode is higher than that of the first eigenmode. In addition,

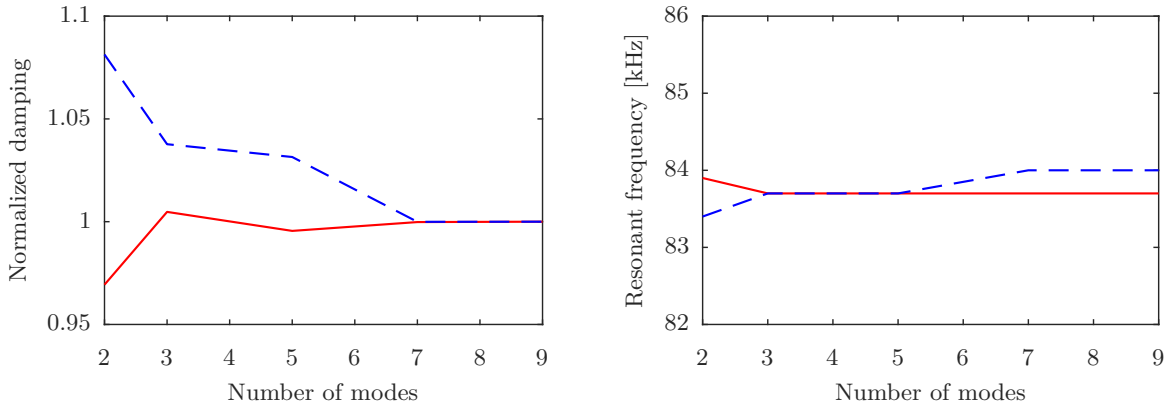

(a) Effect on max. magnitude

(b) Effect on resonant frequency

Figure 7: Convergence analysis of cantilever problem ($\delta = 100\,\mu\text{m}$) with $n_\text{m} \in 2, 3, 5, 7, 9$. Solid lines correspond to the $l = 20\,\text{mm}$ model and dashed lines denote results for the $l = 10\,\text{mm}$ model

a second model is created with a plate segment size of $l = 10\,\text{mm}$. In this configuration, the interfaces are only about three plate thicknesses away from the source. The results for $n_\text{m} = 9$ are shown as dashed lines in Figs. 6(a) and 6(b), and it is seen that the curves are close to those from the 20 mm model.

In a second step, the influence of the number of considered modes is investigated, while keeping the length $l = 20\,\text{mm}$ of the plate segment and the mesh size $\delta = 100\,\mu\text{m}$ constant. For this purpose, the reader is referred to Fig. 5 for the complex wavenumbers and corresponding numbering of the modes. It is commonly assumed that at distances larger than about five times the thickness of the plate ($5 \cdot 2H$) from the source, only the propagating modes are relevant (e.g. [32]). However, as it is shown in Fig. 7, even for the $l = 20\,\text{mm}$ case, at least one additional non-propagating mode needs to be considered for accurate results. At $n_\text{m} = 7$, convergence is achieved. For the $l = 10\,\text{mm}$ model, at least seven modes need to be considered for accurate results. Further increasing the number of considered modes to $n_\text{m} = 9$ does not seem to improve the results. Note that for the convergence graphs in Fig. 7, a maximum of $n_\text{m} = 9$ modes has been considered since the least-square problem does not yield accurate results for a larger number of modes. This is in part due to the fact that the number of unknown wave amplitudes approaches the number of equations.

In order to compare the results from the semi-analytical approaches, a standard transient FE simulation is carried out. A full two-dimensional plane-strain model of the investigated cantilever mounted on a substrate plate is created in Abaqus, however, the substrate plate is created with a length of 1 m such that edge reflections do not interfere with the data of interest within the simulation time. In order to avoid rigid body motion, fixed boundaries are introduced at the left and right edge of the plate, i.e. $\boldsymbol{u} = 0$ at $x = \pm 0.5\,\text{m}$, while all other edges are considered traction free. In order to calculate the transient responses at the reference nodes, Abaqus' explicit time integration mode is used with a fixed time step of 10 ns and a

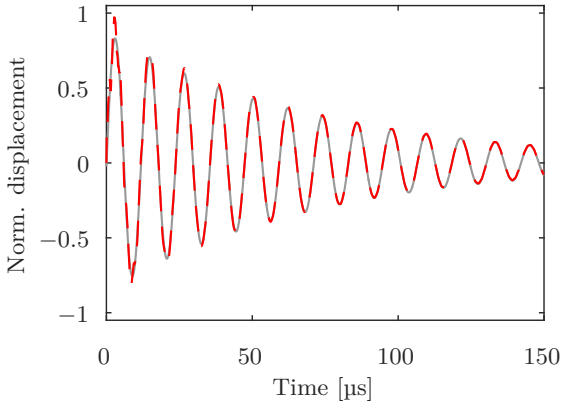

(a) Horizontal displacement $u(t)$ of the left corner node on top of the cantilever

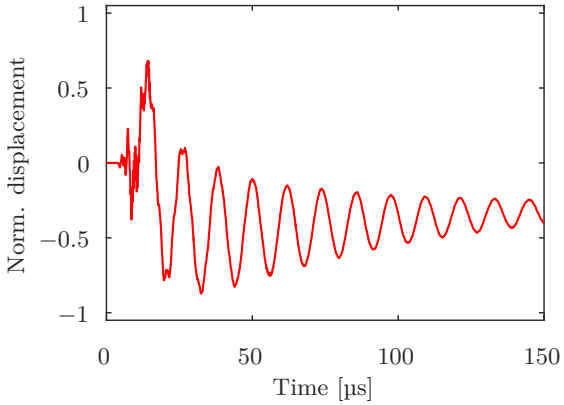

(b) Vertical displacement $v(t)$ of the node at $x = 20\,\text{mm}$ on the top edge of the plate

Figure 8: Transient FE results for cantilever demonstrator are shown as red solid lines. The impulse response of the fitted SDOF system is shown a gray dashed line. Signals are normalized to the maximum value

simulation duration of 150 µs. Meshing parameters are the same (i.e. $\delta = 100\,\mu\text{m}$), however, CPE4 elements are replaced by their CPE4R counterparts for explicit time integration. The horizontal displacement $u(t)$ of the reference node on the cantilever due to an initial velocity that is applied to the top edge of the cantilever is shown in Fig. 8(a) as a red solid line. The first eigenfrequency of the damped cantilever is identified by fitting an SDOF system to the data, resulting in $f = 84.4\,\text{kHz}$ and $\sigma = 14.0\,1/\text{ms}$. The impulse response of the SDOF system is shown as a gray dashed line. In Fig. 8(b), the time history of the vertical displacement $v(t)$ for the node on the substrate plate at $x = 20\,\text{mm}$ is shown. It can be seen that the cantilever induces propagating Lamb waves in the substrate plate. Evaluating the arrival time of the wave front, it can be concluded that mostly antisymmetric waves are induced from the bending of the cantilever.

Results from both the semi-analytical and the transient FE analysis are summarized in Table 1, showing good agreement.

4.2. Double cantilever

Demonstrating the capabilities of the proposed modal analysis approach becomes more evident for a problem for which standard FE methods are less practical. That is, for a high quality factor resonator, energy loss from the resonator into the plate is small and evaluating the transient result would require very long simulation times in order to estimate an accurate decay rate. However, in order to avoid reflections

Table 1: Results for the single cantilever problem

	FRF	Transient	
Eigenfrequency f	83.7	84.4	kHz
Damping σ	14.1	14.0	1/ms

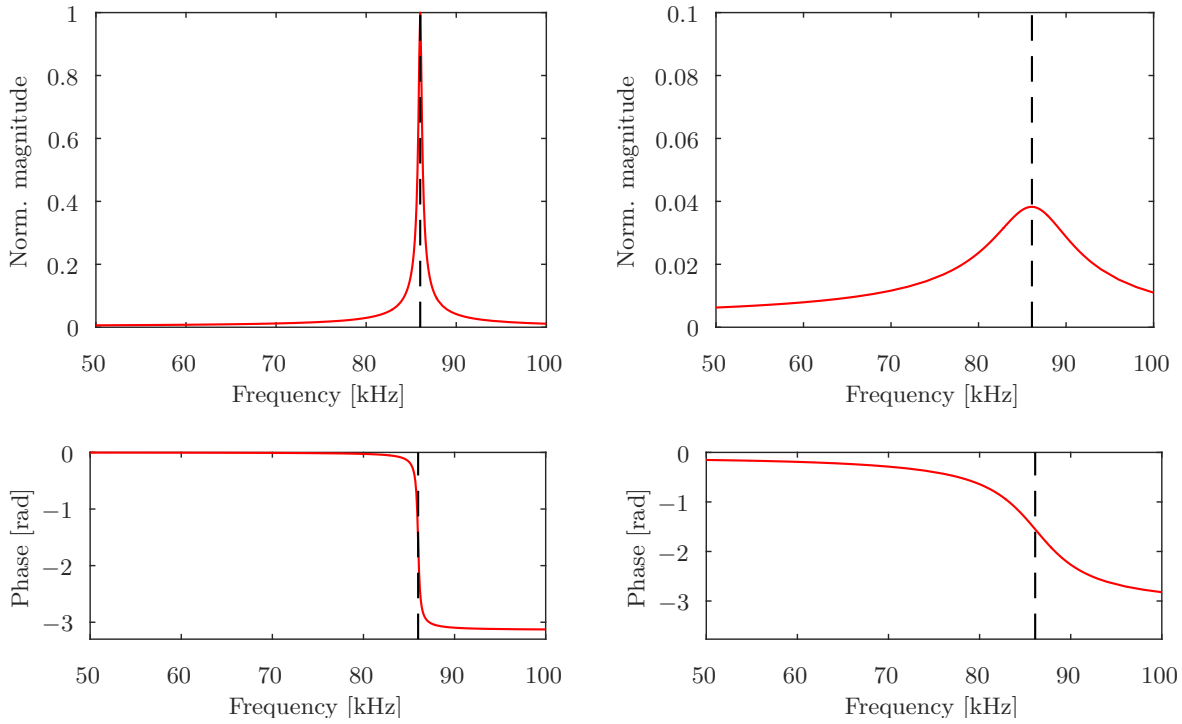

(a) FRF for symmetric loading

(b) FRF for antisymmetric loading

Figure 9: FRF results for double cantilever problem with symmetric (anti-phase) and anti-symmetric loading (in-phase) near first eigenfrequency. Magnitudes are normalized to maximum value

from the ends of the plate, either a very large plate has to be modeled or absorbing boundary conditions have to be implemented [11]. The forced semi-analytical does not suffer from such drawbacks. For the sake of simplicity, the chosen resonator is a double cantilever problem that consists of two identical cantilevers perfectly attached to a substrate plate of the same material, as shown in Fig. 4(b). Geometrical and material parameters are identical to the ones from the previous problem. The distance between the two cantilevers is chosen to be 0.5 mm.

By utilizing the frequency response approach, the FRFs for the top left corner node of the left cantilever are determined for symmetric (anti-phase) loading, as shown in Fig. 4(b), and anti-symmetric (in-phase) loading and are shown in Fig. 9(a) and Fig. 9(b), respectively. Comparing the two results, it can also be seen that anti-symmetric loading causes significantly higher damped vibrations.

In addition, the transient response at the top left corner of the left cantilever to a symmetric (anti-phase) initial velocity field is shown in Fig. 10(a). It can be seen that the anti-phase motion of the cantilevers and their close proximity results in a destructive interference of the induced waves, producing reduced energy loss for this mode of vibration. In other words, the amplitudes of induced propagating Lamb waves are very small. On the other hand, for an antisymmetric (in-phase) initial velocity field, strong damping occurs. The

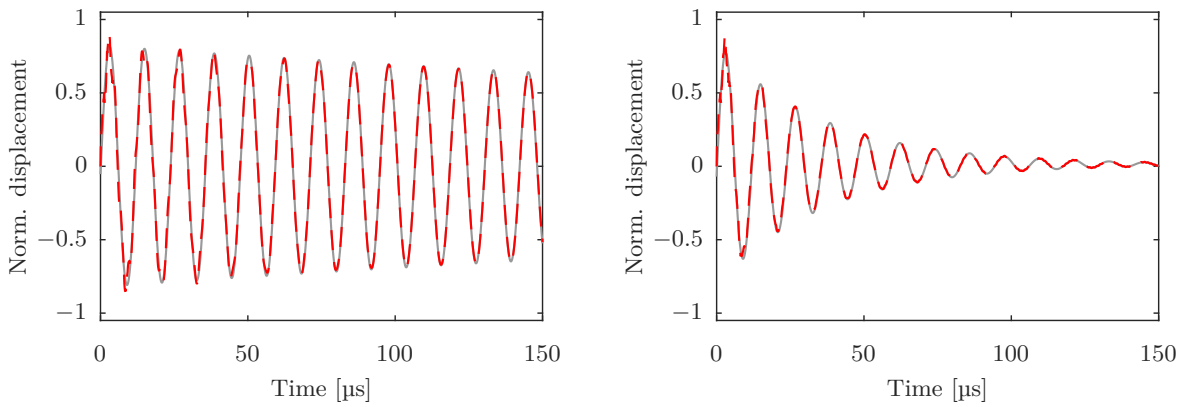

(a) Reponse for symmetric loading

(b) Response for antisymmetric loading

Figure 10: Transient FE results for double cantilever problem with symmetric (anti-phase) and anti-symmetric loading (in-phase) through initial velocity field are shown as red solid lines. Signals are captured at the reference node on the top left corner of the left cantilever and are normalized to maximum value of envelope functions. The impulse responses of fitted SDOF systems are shown as gray dashed lines

transient response for this case is shown in Fig. 10(b).

Comparing the results from both methods, summarized in Table 2, again good agreement can be found.

5. Discussion

Transient FE simulations can be considered the most established method for determining the damping time constants [42]. However, for high quality factor resonators this approach is inadequate due to the fact that the simulated response will not exhibit sufficient decay in amplitude in the reflection-free time interval in order to estimate an accurate value of the damping. Another challenge for the transient simulations is the selection of initial conditions to excite the desired mode. In the cantilever transient simulations (cf. Fig. 8), the initial conditions clearly excite multiple modes despite the fact that the initial conditions were chosen so that a single mode dominated the response. For more complicated resonators, the selection of initial conditions so that the subsequent response is dominated by the mode of interest may not be so

Table 2: Results for the double cantilever problem

	FRF	Transient	
Symmetric (anti-phase) motion			
Eigenfrequency f_s	86.0	84.4	kHz
Damping σ_s	1.1	1.70	1/ms
Anti-symmetric (in-phase) motion			
Eigenfrequency f_a	86.1	84.6	kHz
Damping σ_a	29.6	28.0	1/ms

clear. A related challenge for the semi-analytical steady state analysis is the selection of the forcing term(s) to preferentially excite a given mode. For modes that are well-spaced in frequency, it is straightforward to estimate a quality factor from the frequency response function in a neighborhood of the resonance. However, for modes that are in close proximity, the forcing details and "pick-off" locations can have a large influence on the resulting FRF and so it is more complicated to determine the frequencies and damping values associated with the interacting modes. Furthermore, since the FRF analysis is equivalent to an impulse response calculation, the broadband aspect of the excitation creates frequency response functions that are irrational functions of frequency and, thus, the modal frequency and damping that one associates with an SDOF model can only be an approximation. Nevertheless, from a practical perspective, this is a minor objection since reasonable SDOF responses can be fit to either the transient data or the FRF as was shown in the examples.

6. Concluding remarks

In this paper, a semi-analytical technique for estimating the energy loss in a resonator mounted to a plate substrate has been proposed. The method of stitching together a finite element model and analytical Lamb wave expressions is utilized to generate FRF data to which a SDOF system is fitted in order to approximate modal frequency and damping values. The method has been applied to several plane-strain problems including single- and double-cantilever resonators mounted to thin homogeneous, isotropic plates. By means of this approach, the damping time constants have been directly identified for all investigated eigenfrequencies of the resonator-plate systems. A comparison of the results to those from the semi-analytical frequency response approach and to those from transient FE simulations reveal excellent agreement. Improving the method's computational efficiency will be part of future research, as well its application to more realistic resonator models including three dimensional problems, such as hemispherical resonator gyroscopes.

Acknowledgments

This research was partially supported by DARPA Contract W31P4Q-11-1-0004.

References

[1] M. Weinberg, R. Candler, S. Chandorkar, J. Varsanik, T. Kenny, and A. Duwel1. Energy loss in MEMS resonators and the impact on inertial and RF devices. In *TRANSDUCERS 2009 - 2009 International Solid-State Sensors, Actuators and Microsystems Conference*, pages 688–695, June 2009.

[2] Z. Hao and F. Ayazi. Support loss in the radial bulk-mode vibrations of center-supported micromechanical disk resonators. *Sensors and Actuators A: Physical*, 134(2):582–593, 2007. ISSN 0924-4247. doi: 10.1016/j.sna.2006.05.020.

[3] Z. Hao and Y. Xu. Vibration displacement on substrate due to time-harmonic stress sources from a micromechanical resonator. *Journal of Sound and Vibration*, 322(1âĂŞ2):196–215, 2009. ISSN 0022-460X. doi: 10.1016/j.jsv.2008.11.004.

[4] M. Kanik, P. Bordeenithikasem, D. Kim, N. Selden, A. Desai, R. M'Closkey, and J. Schroers. Metallic glass hemispherical shell resonators. *IEEE J. Microelectromech. Syst.*, 24(1):19–28, Jan 2015.

[5] A. Darvishian, B. Shiari, J. Y. Cho, T. Nagourney, and K. Najafi. Anchor loss in hemispherical shell resonators. *Journal of Microelectromechanical Systems*, 26(1):51–66, Feb 2017. ISSN 1057-7157. doi: 10.1109/JMEMS.2016.2636080.

[6] S. Nitzan, C. H. Ahn, T. H. Su, M. Li, E. J. Ng, S. Wang, Z. M. Yang, G. O'Brien, B. E. Boser, T. W. Kenny, and D. A. Horsley. Epitaxially-encapsulated polysilicon disk resonator gyroscope. In *2013 IEEE 26th International Conference on Micro Electro Mechanical Systems (MEMS)*, pages 625–628, Jan 2013. doi: 10.1109/MEMSYS.2013.6474319.

[7] J. Bernstein, M. Bancu, E. Cook, M. Chaparala, W. Teynor, and M. Weinberg. A MEMS diamond hemispherical resonator. *J. Micromech. Microeng.*, 23(12):1–8, Oct 2013. doi: 10.1088/0960-1317/23/12/125007.

[8] P. Shao, C. Mayberry, X. Gao, V. Tavassoli, and F. Ayazi. A polysilicon microhemispherical resonating gyroscope. *J. Microelectromech. Syst.*, 23(4):762–764, Aug 2014.

[9] J. Y. Cho, J. K. Woo, J. Yan, R. L. Peterson, and K. Najafi. Fused-silica micro birdbath resonator gyroscope (μ-brg). *Journal of Microelectromechanical Systems*, 23(1):66–77, Feb 2014. ISSN 1057-7157. doi: 10.1109/JMEMS.2013.2291534.

[10] D. Senkal, M. J. Ahamed, M. H. A. Ardakani, S. Askari, and A. M. Shkel. Demonstration of 1 million q -factor on microglassblown wineglass resonators with out-of-plane electrostatic transduction. *Journal of Microelectromechanical Systems*, 24(1):29–37, Feb 2015. ISSN 1057-7157. doi: 10.1109/JMEMS.2014.2365113.

[11] D. Binder, E. Quevy, T. Koyama, S. Govindjee, J. Demmel, and R. Howe. Anchor loss simulation in resonators. In *Micro Electro Mechanical Systems, 2005. MEMS 2005. 18th IEEE International Conference on*, pages 133–136, Jan 2005. doi: 10.1109/MEMSYS.2005.1453885.

[12] H. Lamb. On waves in an elastic plate. *Proceedings of the Royal Society of London. Series A, Containing Papers of a Mathematical and Physical Character*, 93(648):114–128, 1917. ISSN 09501207.

[13] P. Kirrmann. On the completeness of Lamb modes. *Journal of Elasticity*, 37(1):39–69, 1994. ISSN 0374-3535. doi: 10.1007/BF00043418.

[14] M. Koshiba, S. Karakida, and M. Suzuki. Finite-element analysis of Lamb wave scattering in an elastic plate waveguide. *IEEE Transactions on Sonics and Ultrasonics*, 31(1):18–25, 1984.

[15] Z. Chang and A. Mal. Scattering of lamb waves from a rivet hole with edge cracks. *Mechanics of Materials*, 31(3):197–204, 1999. ISSN 0167-6636. doi: 10.1016/S0167-6636(98)00060-X.

[16] S. Bischoff, C. Schaal, and L. Gaul. Efficient wave scattering analysis for damaged cylindrical waveguides. *Journal of Sound and Vibration*, 333(18):4203–4213, 2014. ISSN 0022-460X. doi: 10.1016/j.jsv.2014.04.013.

[17] W. Ewing, W. Jardetzky, and F. Press. *Elastic Waves in Layered Media*. McGraw-Hill, New York, 1957.

[18] L. Brekhovskikh. *Waves in Layered Media*. Academic Press, New York, NY, 1960.

[19] J. L. Rose. *Ultrasonic Waves in Solid Media*. Cambridge University Press, New York, NY, 2004. ISBN 978-0521548892.

[20] L. Wang and F. Yuan. Group velocity and characteristic wave curves of Lamb waves in composites: modeling and experiments. *Composites Science and Technology*, 67(7-8):1370–1384, 2007. ISSN 0266-3538. doi: 10.1016/j.compscitech.2006.09.023.

[21] H. Baid, C. Schaal, H. Samajder, and A. Mal. Dispersion of Lamb waves in a honeycomb composite sandwich panel. *Ultrasonics*, 56(0):409–416, 2015. ISSN 0041-624X. doi: 10.1016/j.ultras.2014.09.007.

[22] A. K. Mal and S.-S. Lih. Elastodynamic response of a unidirectional composite laminate to concentrated surface loads: Part I. *Journal of applied mechanics*, 59(4):878–886, 1992.

[23] S.-S. Lih and A. K. Mal. Elastodynamic response of a unidirectional composite laminate to concentrated surface loads: Part II. *Journal of applied mechanics*, 59(4):887–892, 1992.

[24] S.-S. Lih and A. K. Mal. On the accuracy of approximate plate theories for wave field calculations in composite laminates. *Wave Motion*, 21(1):17–34, 1995. ISSN 0165-2125. doi: 10.1016/0165-2125(94)00038-7. Honor and Memory of Julius Miklowitz.

[25] H. Samajder. *Lamb Wave Propagation in Elastic Plates under various loads*. PhD thesis, University of California, Los Angeles, 2015.

[26] D. Placko and T. Kundu. *DPSM for modeling engineering problems*. John Wiley & Sons, Hoboken, NJ, 2007.

[27] B. R. Mace, D. Duhamel, M. J. Brennan, and L. Hinke. Finite element prediction of wave motion in structural waveguides. *The Journal of the Acoustical Society of America*, 117(5):2835–2843, 2005. doi: 10.1121/1.1887126.

[28] C. Schaal and A. Mal. Dispersion of guided waves in composite laminates and sandwich panels. *Proc. SPIE*, 9438: 94380L–1–94380L–12, 2015. doi: 10.1117/12.2083870.

[29] C. Schaal, S. Tai, and A. Mal. On the assumption of transverse isotropy of a honeycomb sandwich panel for NDT applications. *Proc. SPIE*, 10170:1017022–1017022–8, 2017. doi: 10.1117/12.2260092.

[30] L. Gavrić. Computation of propagative waves in free rail using a finite element technique. *Journal of Sound and Vibration*, 185(3):531–543, 1995. ISSN 0022-460X. doi: 10.1006/jsvi.1995.0398.

[31] S. Finnveden. Spectral finite element analysis of the vibration of straight fluid-filled pipes with flanges. *Journal of Sound and Vibration*, 199(1):125–154, 1997. ISSN 0022-460X. doi: 10.1006/jsvi.1996.0602.

[32] N. Vasudevan and A. Mal. Response of an elastic plate to localized transient sources. *Journal of Applied Mechanics*, 52 (2):356–362, 1985. doi: 10.1115/1.3169053.

[33] A. K. Mal and S. J. Singh. *Deformation of Elastic Solids*. Prentice Hall New Jersey, 1991.

[34] C. Schaal, H. Samajder, H. Baid, and A. Mal. Rayleigh to Lamb wave conversion at a delamination-like crack. *Journal of Sound and Vibration*, 353(0):150–163, 2015. ISSN 0022-460X. doi: 10.1016/j.jsv.2015.05.016.

[35] D. C. Gazis and R. D. Mindlin. Extensional vibrations and waves in a circular disk and a semi-infinite plate. *Journal of applied mechanics*, 27(3):541–547, 1960.

[36] P. J. Torvik. Reflection of wave trains in semi-infinite plates. *The Journal of the Acoustical Society of America*, 41(2): 346–353, 1967. doi: 10.1121/1.1910344.

[37] C. Schaal and A. Mal. Lamb wave propagation in a plate with step discontinuities. *Wave Motion*, 66:177–189, 2016. ISSN 0165-2125. doi: 10.1016/j.wavemoti.2016.06.012.

[38] C. Schaal, S. Bischoff, and L. Gaul. Analysis of wave propagation in periodic 3D waveguides. *Mechanical Systems and*

Signal Processing, 40(2):691–700, 2013. ISSN 0888-3270. doi: 10.1016/j.ymssp.2013.06.021.

[39] E. Glushkov, N. Glushkova, and O. Lapina. Diffraction of normal modes in composite and stepped elastic waveguides. *Journal of Applied Mathematics and Mechanics*, 62(2):275–280, 1998. ISSN 0021-8928. doi: 10.1016/S0021-8928(98)00035-5.

[40] M. A. Flores-López and R. Douglas Gregory. Scattering of Rayleigh-Lamb waves by a surface breaking crack in an elastic plat. *The Journal of the Acoustical Society of America*, 119(4):2041–2049, 2006. doi: 10.1121/1.2180209.

[41] Y. Al-Nassar, S. Datta, and A. Shah. Scattering of lamb waves by a normal rectangular strip weldment. *Ultrasonics*, 29 (2):125–132, 1991. ISSN 0041-624X. doi: 10.1016/0041-624X(91)90041-6.

[42] K.-J. Bathe. *Finite element procedures*. Klaus-Jurgen Bathe, Cambridge, MA, 2006. ISBN 978-0979004902.